Nigerian Research Journal of Engineering and Environmental Sciences 4(1) 2019 pp. 27-40

Nigerian Research Journal of Engineering and Environmental Sciences
Journal homepage: www.rjees.com

Original Research Article

Numerical Modelling of Laminar Flows in a Rectangular Microchannel

Ismail, O.S. and *Abu, K.
Department of Mechanical Engineering, Faculty of Technology, University of Ibadan, Nigeria.
*abukareemid@yahoo.com

ARTICLE INFORMATION

Article history:
Received 25 February, 2019
Revised 14 April, 2019
Accepted 18 April, 2019
Available online 30 June, 2019

Keywords:
Laminar flow
Microchannel
Navier-Stokes equations
Reynolds number
Numerical stability

ABSTRACT

Numerical solution of laminar flow of water in a microchannel of rectangular cross-section of 10 mm by 10 mm is presented in this work for Reynolds number (Re) ranging from 10 to 300. The unsteady incompressible Navier-Stokes equations were discretised using the finite difference method, solved using the pressure-projection approach and then implemented with the code written with MATLAB. The code was validated with analytical and ANSYS Fluent solution of channel flow. Pressure was greatest at the inlet near corners of the microchannel, and continually reduced downstream. The velocity at a median vertical section along the flow channel varied parabolically, increasing from zero at the walls to the maximum value at the central axis of the channel. The Courant number evaluated for each case of Re was less than 1, ensuring the numerical stability of the code. The present work can thus be used to visualise velocity and pressure distribution in a microchannel.

1. INTRODUCTION

The small characteristic dimensions of microchannels cause low flow velocity, an important feature of laminar flows, which promotes fouling in microfluidic devices such as in microheat exchangers thus raising issues bordering on cleaning (Cengel, 2004; Wilson, 2005; Bode *et al.*, 2007 Brandner *et al.*, 2007). Details about the theory of laminar flow can be found in Batchelor (2000). Furthermore, laminar flow in microfluidic devices provides a clue to biochemical processes taking place in living things (Jenkins and Mansfield, 2013; Li and Zhou, 2013). Besides, laminar flow enables the production of microbial fuel cells without the use of physical membrane barrier (Li *et al.,* 2011; Angenent *et al.,* 2012; Wang and Su, 2013; Fraiwan *et al.,* 2014). Authors like Qi *et al.* (2008) and *Zhang et al.* (2005) have conducted separate investigations to highlight the importance of laminar flow through channels of different cross-sections in the areas of cleaning fluidic devices and transport of blood in veins respectively. Qi *et al.* (2008) investigated effects such as local wall shear stress enhancement, flow reversal and phase shift/angle of laminar pulsed flow of incompressible Newtonian fluid through rectangular microchannels using the Green functions under two types of pressure gradients—time-sinusoidal pressure gradient super-imposed on a constant one and delayed triangular pressure gradient superimposed on a constant one. They concluded that the normalised shear stress under

periodic delayed triangular pressure gradient with long pulse live time is slightly higher than for short pulse live time, indicating an enhancement of wall shear stress which is applicable in the cleaning of microchannels.

In another report, Kim (2016) conducted an experimental study to clarify some discrepancies involved in fluid flow and heat transfer using rectangular microchannels of hydraulic diameter d_h = 155 – 580μm, aspect ratios of 0.25 – 3.8 at Re ranging from 30 to 2500 and FC770 (a type of deionised water) as the working fluid. Pressure drop along the microchannel increased as the mass flow rate increased. It was reported that single-phase laminar friction factors in the microchannels agreed well with the conventional Poiseuille flow theory, and that critical Re increased from 1700 to 2400 as the aspect ratio decreased from 1.0 to 0.25. It was concluded that experimental Nusselt number (Nu) values were lower than the theoretical values at Re < 180, and assessed that the theoretical Nu at Re > 180 were reasonable estimates when aspect ratio > 1.0. In physiology, the ability of a vessel such as the artery to increase in volume with pressure is the vessel compliance. Zhang *et al.* (2005) conducted numerical investigation of two-dimensional steady laminar flow for rectangular channel with compliant wall for Reynolds number ranging from 1 – 400. They solved the Navier-Stokes equation using the finite volume method, the membrane equation governing the compliant wall using finite difference method and coupled the solutions iteratively using spring analogy smoothing technique. They presented the shapes of compliant walls at the various Re for certain pressure-scaling factor and tension-scaling factor, and reported that pressure drop within the channel increased as Re increased.

In order to understand pressure drop in porous channel, Sandeep (2001) derived analytical expressions for rectangular slit as well as cylindrical tube with constant wall permeability, for which pressure drop was found to be a function of channel dimension, wall permeability, axial position and the fluid viscosity. The study proposed benchmark numerical routines for fluid flow modelling past semi-permeable membranes and for making quick engineering estimates for pressure drop in cross-flow membrane modules. Raja *et al.* (2009) numerically studied the behaviour of laminar incompressible jet flow for Re ranging from 300 to 600 and Grashof number (Gr) = $10^3 – 10^7$. They solved the unsteady vorticity transport equation using alternating direct implicit (ADI) scheme and the energy equation. They presented the horizontal velocity profile at different locations of the flow domain, Re and Gr, and observed that the velocity decreased in the downstream direction for Gr = 10^3 and 10^4 where forced convection dominated (i.e. Richardson number Ri = Gr/Re^2 was small), while at Gr = 10^7, the offset jet was primarily buoyant jet regardless of Re. Nusselt number Nu was reported to decrease with decrease in Gr for a particular Re, but increased with increase in Gr at the respective Re. They concluded that re-attachment length strongly depended on Re and Gr.

Regarding flow in curved duct, Papadopoulos (2011) developed a novel auxiliary potential velocity scheme for incompressible flows and implemented it on curved circular ducts and a set of benchmark problems to validate the accuracy and convergence of the scheme. The scheme was used to determine the axial velocity profiles in curved circular duct of curvature k = 0.05 at Re = 4000, Dean number (De) = 894 as well as Re = 2800, De =626, both of which are parabolic in shape. The pressure drop which increased along the horizontal diameter of the curved circular duct was also presented. Details of flow in curved ducts can be found in Mees *et al.* (1996) and Berger *et al.* (1983). Furthermore, in view to understanding laminar flowin helical duct other than curved duct, Morales and Rosa (2012) investigated laminar flow in helical duct of rectangular cross-section and constant pitch. They solved the transport equations in orthogonal coordinates, based on Germano transformation, and on staggered mesh using finite-volume method and interpolation scheme for the convective terms. The effects of torsion τ, curvature $\kappa$and hydraulic diameter $d_h$on the velocity profiles and friction factor were examined, having good agreement with experimental data, with 4.83% error on maximum Re and 1% error on the average wall friction factor. It was concluded that the approach could be used for formulation of helical ducts of a square cross section for $\tau.d_h \leq 0.4$ and $\kappa.d_h < 0.471$.

Many authors have endeavoured to develop schemes for solving the Navier-Stokes equation, taking into consideration accuracy, convergence rate and computational time. In one of the pioneering works, Spalding

and Patankar (1972) developed the SIMPLE algorithm for solving mass transport, flow and heat transfer problems. Other derivatives of SIMPLE include SIMPLER and fully implicit Coupled and Linked equations Algorithm Revised (CLEAR). Tao *et al.* (2004a; 2004b) presented CLEAR, with an enhanced rate of convergence, as a review of the SIMPLER algorithm. In this paper we present the variation of velocity and pressure in laminar flow by solving two- dimensional unsteady Navier-Stokes equations via finite difference method on staggered grid and using the pressure-projection method. This approach is adopted because of its simplicity and fast convergence without any need for relaxation factor. This formulation is applied to two-dimensional rectangular ducts.

2. METHODOLOGY

2.1. Problem Description

Consider a rectangular channel of dimension *w* x *h*, where *w* is the width and *h* is the height (Figure 1). Water flows into the channel through the inlet (left face) with velocity U_{in}.

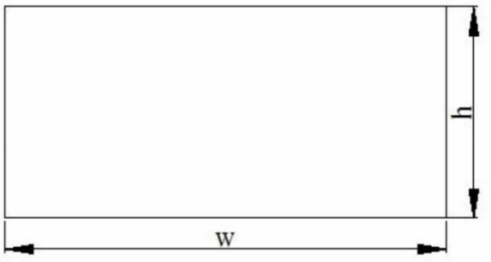

Figure 1: Two dimensional microchannel

The Reynolds number based on *h* is given as:

$$Re = \frac{U_{in}h}{\nu} \tag{1}$$

where ν is the kinematic viscosity of water. The temperature of the fluid is assumed to be uniform so that viscosity remains constant. The velocity and pressure distribution at various Reynolds numbers 10, 20, 30, 50, 100, 200 and 300 were determined.

2.2. Governing Equations and Boundary Conditions

The transport equations of two dimensional incompressible Eularian fluid flow are given as follows (Versteeg and Malalasekera, 2007). Equation 2 represents continuity while Equations 3 and 4 give the x-momentum and y-momentum respectively.

$$\frac{\partial u}{\partial x} + \frac{\partial v}{\partial y} = 0 \tag{2}$$

$$\frac{\partial u}{\partial t} + \frac{\partial u^2}{\partial x} + \frac{\partial uv}{\partial y} = -\frac{\partial P}{\partial x} + \nu\left(\frac{\partial^2 u}{\partial x^2} + \frac{\partial^2 u}{\partial y^2}\right) \tag{3}$$

$$\frac{\partial v}{\partial t} + \frac{\partial uv}{\partial x} + \frac{\partial v^2}{\partial y} = -\frac{\partial P}{\partial y} + \nu\left(\frac{\partial^2 v}{\partial x^2} + \frac{\partial^2 v}{\partial y^2}\right) \tag{4}$$

where u = horizontal component of velocity, v = vertical component of velocity, P = p/ρ, i.e. the pressure per unit density and ν is the kinematic viscosity.

The flow through the channel is considered to be laminar, incompressible in which temperature throughout the flow field is uniform, so that viscosity is constant.

The following boundary conditions (Figure 2) were used along with the governing differential equations.

Inflow: $u = U_{in}; v = 0; \frac{\partial p}{\partial y} = 0$

Outflow: $\frac{\partial u}{\partial x} = \frac{\partial v}{\partial y} = 0; p = 0$

Wall (Top and bottom): $u = \ v = 0; \ \frac{\partial p}{\partial x} = 0$

2.3. Grid Formulation

In finite difference method, the derivatives are replaced with differences. In Figure 2, *i-j* set of cell counters were employed in the grid formation, with *i* representing the cell number in the horizontal direction and j representing cell number in the vertical direction. The resulting 2-D array of zones, called *mesh* is made up of *ix j* individual small rectangles of *dx* and height *dy*. The pressure per unit density is represented at the cell centres, horizontal velocity at the right and left walls or faces of the cells, and vertical velocity at the top and bottom cell walls. P = pressure per unit density, u = horizontal velocity, and v = vertical velocity as shown in the staggered grid in Figure 3.

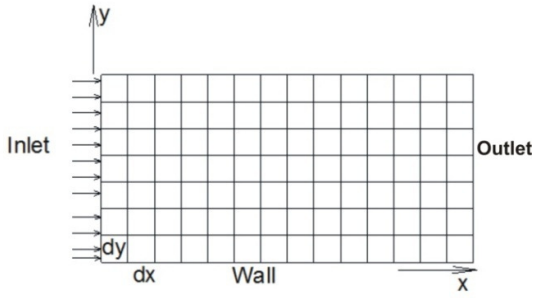

Figure 2: Two-dimensional mesh (with the boundaries)

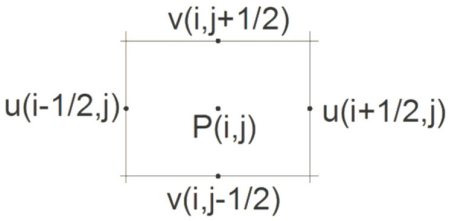

Figure 3: The staggered mesh

2.4. Numerical Procedure using Finite Difference

To solve the equations of two-dimensional incompressible fluid flow, a method that combines both explicit and implicit techniques are employed to cater for stability condition that is present in the pressure term of the momentum equations. The advective and viscous terms are discretised using explicit finite difference method, while the change in pressure is calculated using implicit method.

Equations 3 and 4 were re-written such that the advective terms and viscous terms are grouped.

$$\frac{\partial u}{\partial t} = \left[-\frac{\partial u^2}{\partial x} - \frac{\partial uv}{\partial y} + \nu\left(\frac{\partial^2 u}{\partial x^2} + \frac{\partial^2 u}{\partial y^2}\right)\right] - \frac{\partial P}{\partial x} \quad (5)$$

$$\frac{\partial v}{\partial t} = \left[-\frac{\partial uv}{\partial x} - \frac{\partial v^2}{\partial y} + \nu\left(\frac{\partial^2 v}{\partial x^2} + \frac{\partial^2 v}{\partial y^2}\right)\right] - \frac{\partial P}{\partial y} + g_y \tag{6}$$

$$\text{Let } B = \left(u\frac{\partial u}{\partial x}\right)_{i,j}, C = \left(u\frac{\partial v}{\partial y}\right)_{i,j}, E = \left(\frac{\partial 2_u}{\partial x^2}\right)_{i,j}, F = \left(\frac{\partial 2_u}{\partial y^2}\right)_{i,j} \tag{7}$$

Using finite difference method to discretise the differentials, forward difference was applied to first derivative in space and unsteady term while second order symmetric difference was applied to the second-order derivative in space.

Therefore, B, C, E and F are expressed as follows.

$$\left.\begin{aligned} B &= \frac{u(i,j)[u(i+1,j)-u(i-1,j)]}{2\Delta x} \\ C &= \frac{v(i,j)[u(i,j+1)-u(i,j-1)]}{2\Delta y} \\ E &= \frac{u(i-1,j)-2u(i,j)+u(i+1,j)}{(\Delta x)^2} \\ F &= \frac{u(i,j-1)-2u(i,j)+u(i,j+1)}{(\Delta y)^2} \end{aligned}\right\} \tag{8}$$

$$\left(\frac{\partial u}{\partial t}\right)_{i,j}^{n} = \frac{u_{i,j}^{n+1}-u_{i,j}^{n}}{\Delta t} \tag{9}$$

$$\left(\frac{\partial p}{\partial x}\right)_{i,j} = \frac{p(i+1,j)-p(i,j)}{\Delta x} \tag{10}$$

$$\therefore \left(\frac{\partial u}{\partial t}\right) = -B - C + \nu(E+F) - \frac{1}{\rho}\left(\frac{\partial p}{\partial x}\right) \tag{11}$$

Substituting for B, C, E and F in Equation (11) from the Equation set (8), we have:

$$u_{i,j}^{n+1} = u_{i,j}^{n} + \Delta t(-B - C + \nu(E+F) - \frac{(\Delta t)}{\rho}\left[\frac{p(i+1,j)-p(i,j)}{\Delta x}\right]$$

$$\Longrightarrow u_{i,j}^{n+1} = u_{i,j}^{n} + \text{fu} - \left(\frac{\Delta t}{\Delta x}\right)[P(i+1,j) - P(i,j)]$$

We write NS_fu $= -B - C + \nu(E+F)$ so that fu = (Δt)NS_fu.

An Intermediate u-velocity u_{int} is defined such that:

$$u_{int}(i,j) = u_{i,j}^{n} + \text{fu} \tag{12}$$

$$\text{So that: } u_{i,j}^{n+1} = u_{int}(i,j) - \left(\frac{\Delta t}{\Delta x}\right)[P(i+1,j) - P(i,j)] \tag{13}$$

Equation (13) represents the discretised x-momentum equation. Similarly, the discretised y-momentum equation is obtained thus.

$$\left.\begin{aligned} G &= u(i,j)\frac{v(i+1,j)-v(i-1,j)}{2\Delta x} \\ H &= v(i,j)\frac{v(i,j+1)-v(i,j-1)}{2\Delta y} \\ L &= \frac{v(i-1,j)-2v(i,j)+v(i+1,j)}{(\Delta x)^2} \\ M &= \frac{v(i,j-1)-2v(i,j)+v(i,j+1)}{(\Delta y)^2} \end{aligned}\right\} \quad (14)$$

$\mathrm{NS_{fv}} = -G - H + \nu(L + M) - g;$

fv = (Δt)NS_fv

$$\therefore \mathrm{v}_{int}(\mathrm{i},\mathrm{j}) = v_{i,j}^{n} + \mathrm{fv} \quad (15)$$

Where v_{int} is an intermediate v-velocity

$$v_{i,j}^{n+1} = \mathrm{v}_{int}(\mathrm{i},\mathrm{j}) - \left(\frac{\Delta t}{\Delta y}\right)[P(i,j+1) - P(i,j)] \quad (16)$$

To achieve convergence, quantity $D_{i,j}$ is defined in Equation (17). But this value might not be zero at the start of the iteration. Therefore, the residual of $D_{i,j}$ is monitored to evaluate how the values are converging.

$$D(i,j) = \frac{u(i+1,j)-u(i,j)}{\Delta x} + \frac{v(i,j+1)-v(i,j)}{\Delta y} \quad (17)$$

Using Newton Raphson method, pressure is written as in Equation (18).

$$P_{i,j}^{new} = P_{i,j}^{old} - \frac{D(P_{i,j}^{old})}{\left(\frac{\partial D}{\partial P}\right)_{i,j}} \quad (18)$$

$(\partial D/\partial P)_{i,j}$ is calculated using chain rule.

For function y = f(a(x),b(x),..), we can write chain rule as:

$$\frac{\partial y}{\partial x} = \frac{\partial f}{\partial a}.\frac{\partial a}{\partial x} + \frac{\partial f}{\partial b}.\frac{\partial b}{\partial x} + \cdots$$

$$\therefore \left(\frac{\partial D}{\partial P}\right)_{i,j} = \frac{\partial D_{i,j}}{\partial u_{i+1,j}} \cdot \frac{\partial u_{i+1,j}}{\partial P_{i,j}} + \frac{\partial D_{i,j}}{\partial u_{i-1,j}} \cdot \frac{\partial u_{i-1,j}}{\partial P_{i,j}} + \frac{\partial D_{i,j}}{\partial \mathrm{v}_{i,j+1}} \cdot \frac{\partial \mathrm{v}_{i,j+1}}{\partial P_{i,j}} + \frac{\partial D_{i,j}}{\partial \mathrm{v}_{i,j-1}} \cdot \frac{\partial \mathrm{v}_{i,j-1}}{\partial P_{i,j}} \quad (19)$$

Substituting Equations 13, 16 and 17 into Equation 19, Equation 20 is obtained.

$$\left(\frac{\partial D}{\partial P}\right)_{i,j} = \frac{1}{\Delta x}\left(\frac{\Delta t}{\Delta x}\right) + \left(-\frac{1}{\Delta x}\right)\left(-\frac{\Delta t}{\Delta x}\right) + \frac{1}{\Delta y}\left(\frac{\Delta t}{\Delta y}\right) + \left(-\frac{1}{\Delta y}\right)\left(-\frac{\Delta t}{\Delta y}\right) = 2\Delta t\left(\frac{1}{\Delta x^2} + \frac{1}{\Delta y^2}\right) \quad (20)$$

Consequently, the equation for the implicit-updating of pressures is:

$$P_{i,j}^{new} = P_{i,j}^{old} - \beta D_{i,j} \quad (21)$$

$$\text{Where } \beta = \frac{1}{2\Delta t\left(\frac{1}{\Delta x^2} + \frac{1}{\Delta y^2}\right)} \quad (22)$$

The flow chart in Figure 4 summarises the computational solution in three stages: pre-processor stage, solver stage and post-processor stage.

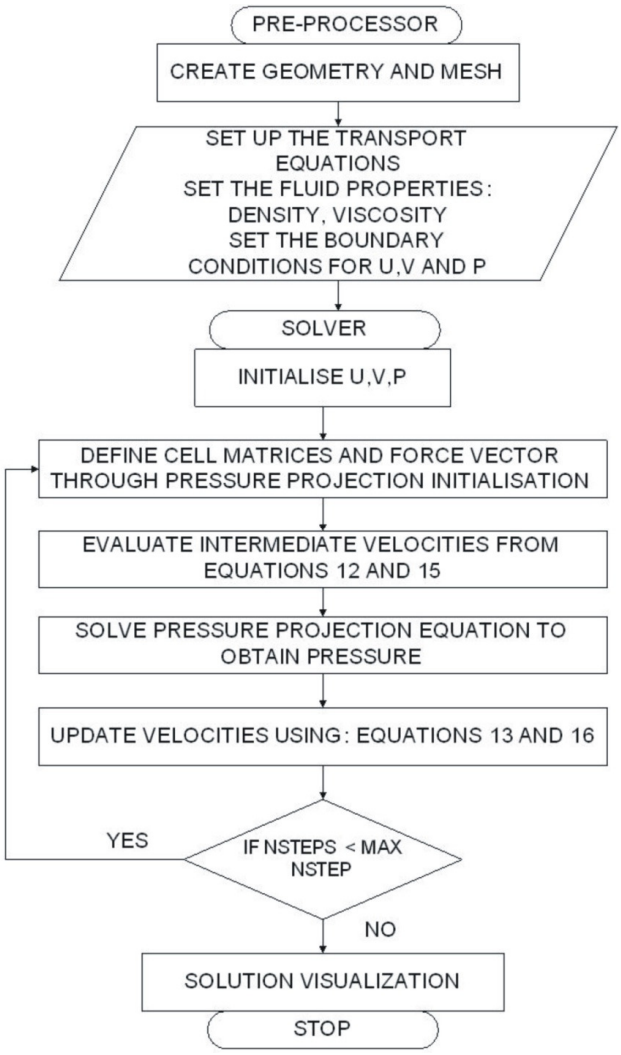

Figure 4: Flow chart for computational solution

2.5. Mesh Dependency

The size of grid as well as the number of grids defines the mesh used in numerical simulation. The mesh size influences the result accuracy and computational time. The finer the mesh, the more time required to complete the simulation. Therefore, an attempt is made to determine the grid size that is just suitable for the simulation, ensuring good accuracy of the results and minimising the computational time. Simulation results at $Re_h = 10$ with meshes 20 x 20 and 50 x 50 are presented in Figure 5.

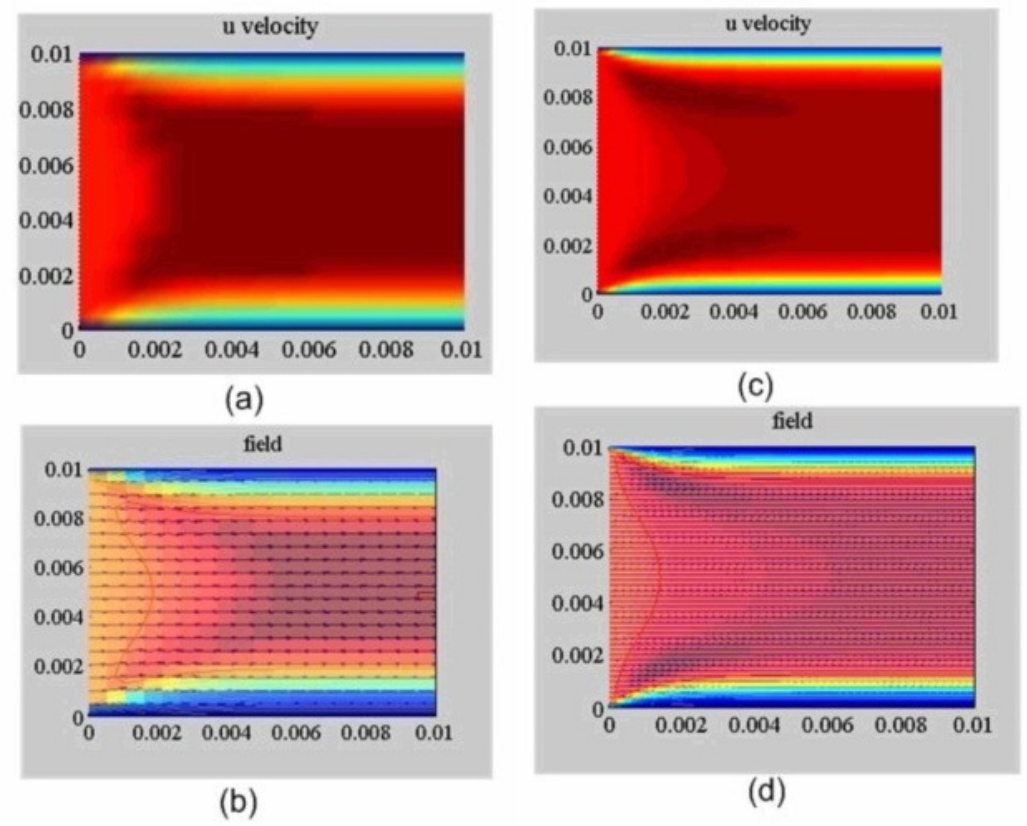

Figure 5: Laminar flow development along the rectangular channel at Re_h=10: (a, b) mesh 20x20; (c, d) mesh 50x50

Figures 5c and 5d use 50 x 50 mesh and give a more vivid picture of the laminar velocity profile as being parabolic than Figures5a and 56b. With mesh 20 x 20 used for Re_h = 20, average simulation time is 1 minute 50 seconds while 50 x 50 mesh with the same Re_h results in average simulation time of 7 minutes 25 seconds on HP Compaq Presario CQ61 computer running on 32-bit Windows Operating System. We adopt mesh 50 x 50 because it offers better visualisation of the velocity profile than mesh 20 x 20, though its simulation time is over four times of the latter.

3. RESULTS AND DISCUSSION

3.1. Validation

The numerical procedure developedin this work is validated by comparison with the analytical solution of channel flow governed by$u = u_{max}(1 - \left(\frac{r}{R}\right)^2)$) (White, 1998) obtained using ANSYS Fluent. Figure 6a presents the u-velocity profile which agrees well with the analytical solution in Figure 6b such that mid downstream, the velocity fields are each approximately 1.5 x 10^{-3} m/s. Both figures show that the u-velocity increases from zero at the walls to the maximum at the central horizontal axis through the channel.

Figures 7a and 7b illustrate that there is higher pressure developed at the wall corner near the inlet, and that the pressure drop increases downstream the channel.

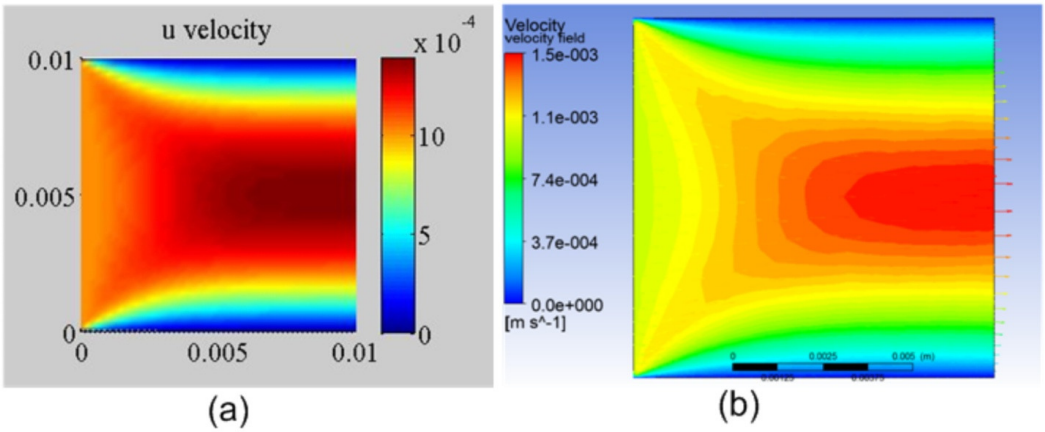

Figure 6: u-velocity along the flow channel: (a) present work at Re_h= 10; (b) ANSYS Fluent solution

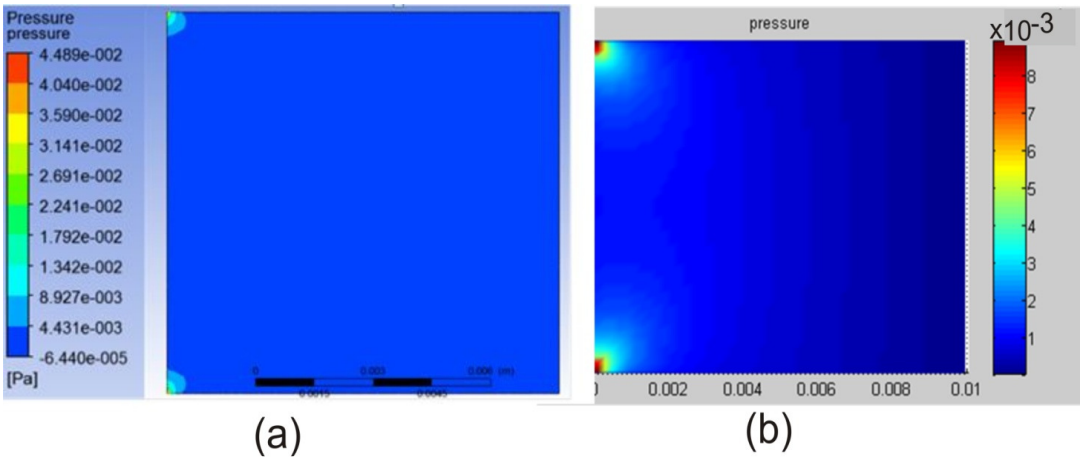

Figure 7: Pressure distribution in the channel: (a) ANSYS Fluent; (b) present work at Re_h = 10

3.2. Velocity and Pressure Distribution at Different Reynolds Numbers

The flow visualisation obtained for Re_h = 20, 30, 40, 50 and 100 are presented in Figures 8, 9, and 10. The flow distributions in the Figures 8d-f, 9 and 10 have similar profiles as Figures 8a-c. Figure 8a shows the velocity distribution downstream at Re = 20. It illustrates the velocity as increasing from the entry to maximum value towards the centre of the flow domain. Figure 8b depicts the fluid layers as they progress downstream without crossing each other. The far downstream curve coincides approximately with the middle of the channel, and this is expectedly the hydrodynamic length (l_e). Figure 8c gives the pressure distribution within the channel, in which pressure is highest at the inlet corners, and least at the exit. A common observable characteristic in the flow pattern shown in Figures 8e, 9b, 9e and 10b is that the parabolic curve far downstream is well beyond the middle of the channel by about 5% of the channel length w for $30 \leq Re \leq 100$.

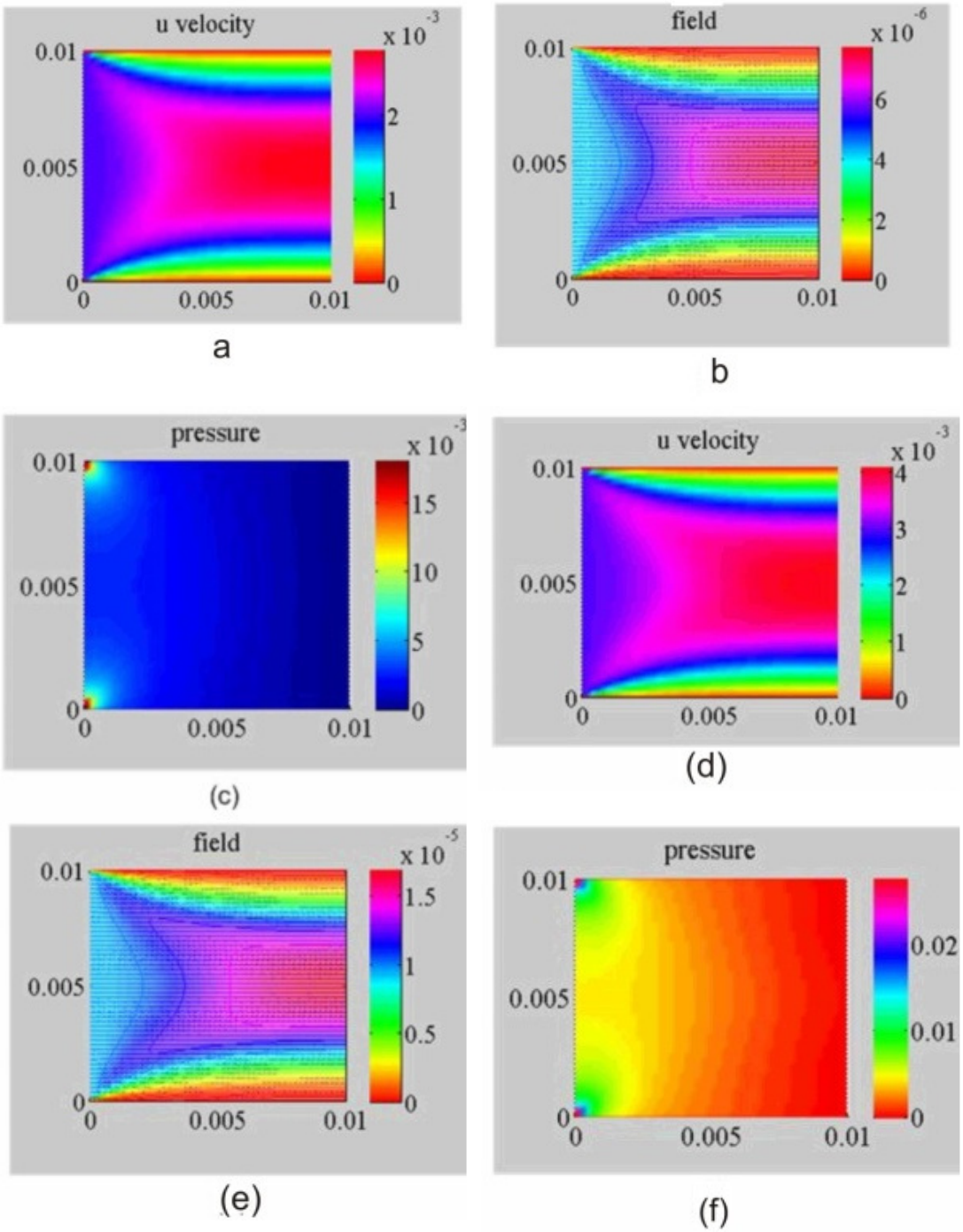

Figure 8: Velocity and pressure distribution: (a-c) Re_h = 20; (d-f) Re = 30

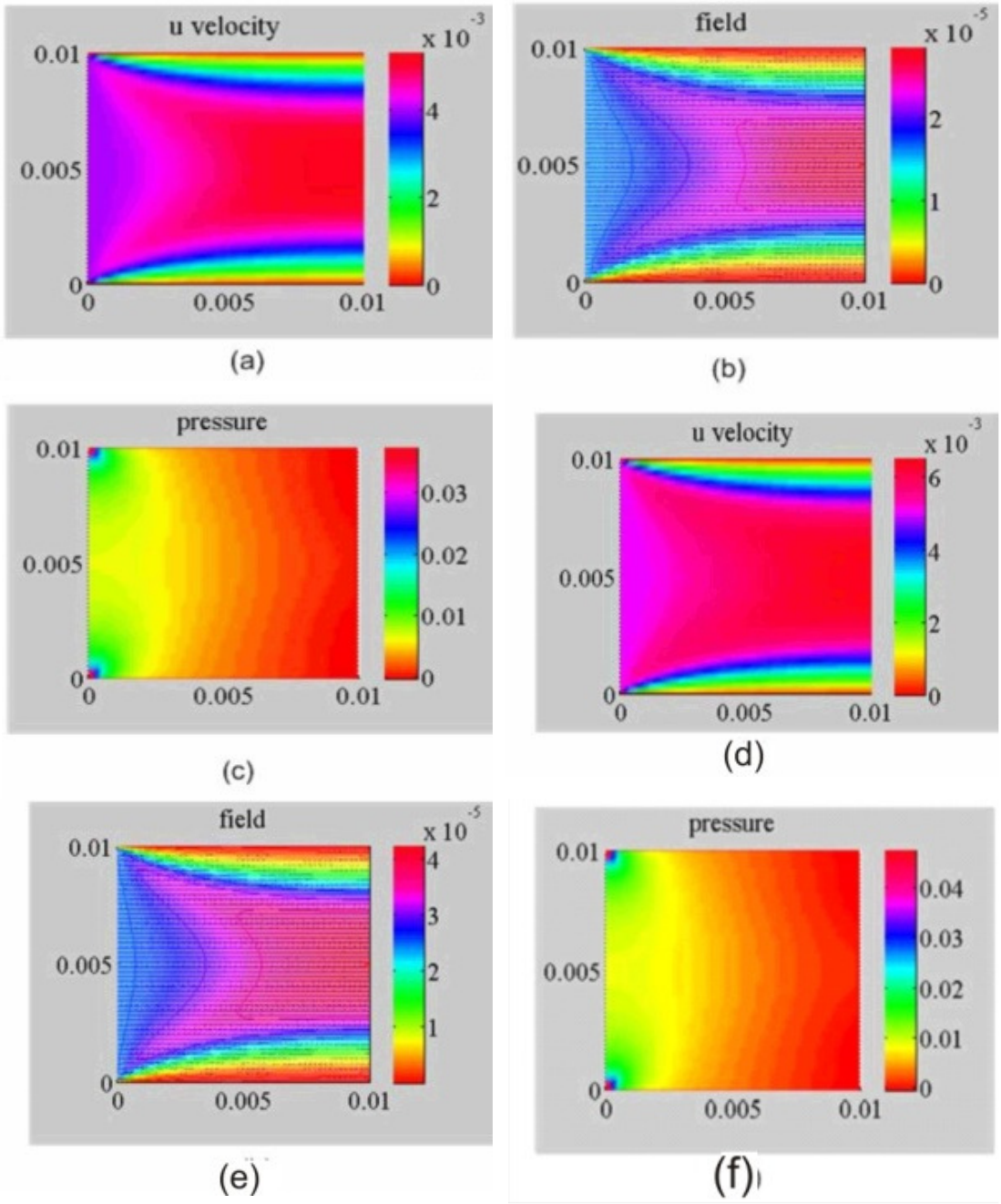

Figure 9: Velocity and pressure distribution: (a-c) Re_h = 40; (d-f) Re = 50

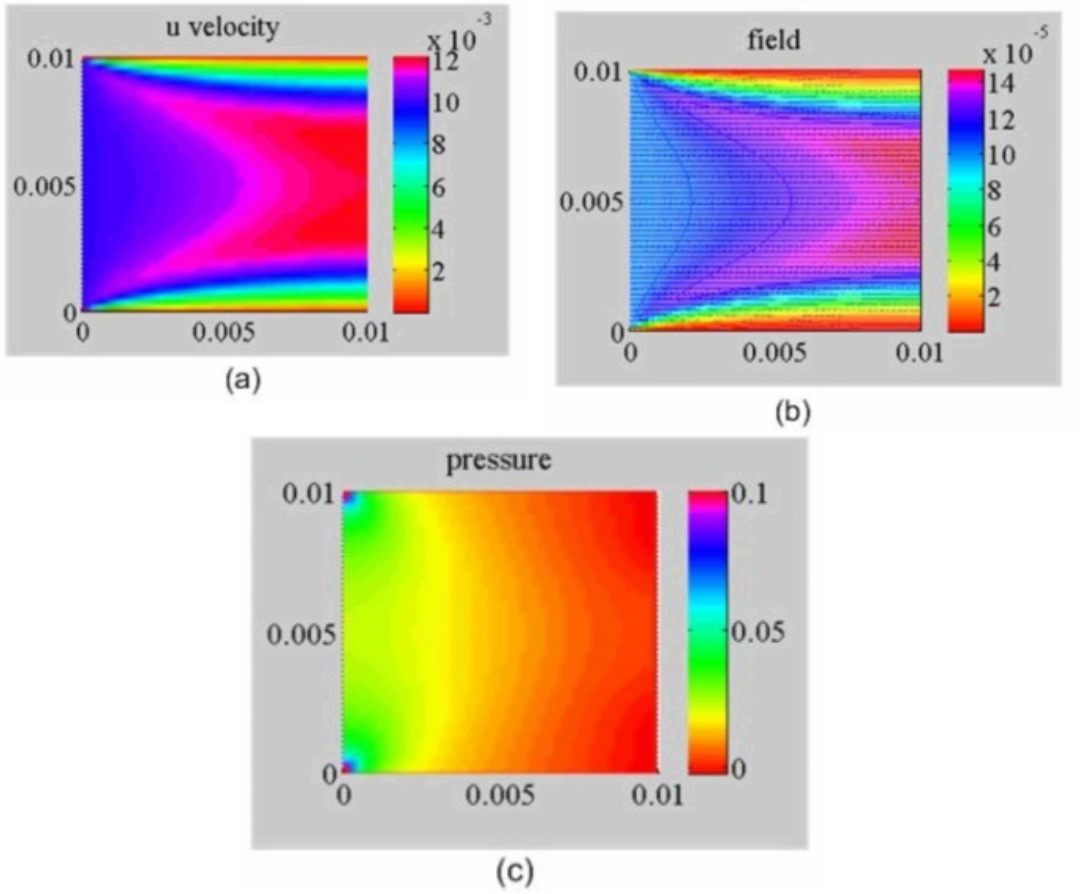

Figure 10: u-velocity and pressure distribution at Re_h= 100

The numerical formulation presented in this work can capture the effects of Reynolds number on velocity distribution up to Re = 300. Figures 11a and 11b show laminar flow distribution at Re = 200 and 300 respectively. Figure 11a shows flow patterns that are similar that of Figure 8b in that the far downstream curve (in Figure 11a) is formed where the hydrodynamic length (l_e) is about half of the channel length (w). However, the far downstream curve in Figure 11b is formed where l_e<0.5w by 0.05w.

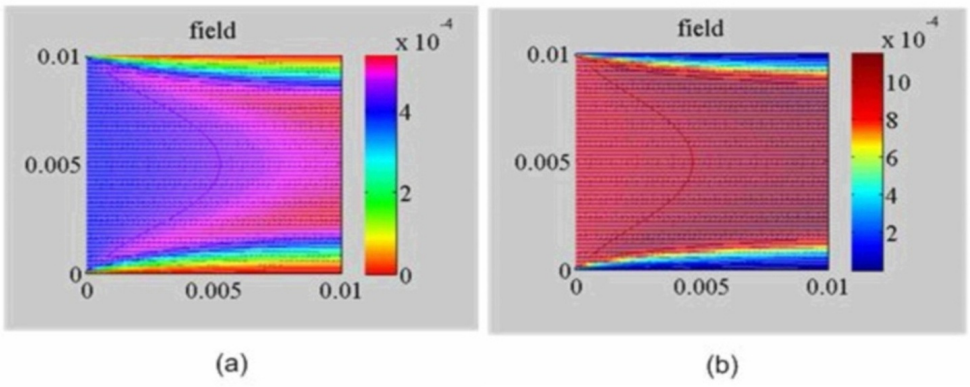

Figure 11: (a)Velocity field at Re = 200; (b) velocity field at Re = 300

3.3. Numerical Stability

The numerical stability of the finite-difference formulation, in terms of Courant number (Co) and Peclet number was checked for the aforementioned Reynolds number and presented in Table 1. Table 1 presents the maximum cell Reynolds number, the Courant number values and Maximum Cell Peclet number at various Re_h The Peclet number is used for monitoring convection-diffusion phenomenon and continuity. The Courant numbers obtained for the horizontal and vertical components of velocity (Co_u, Co_v respectively) were less than 1 for each simulation case, ensuring that the numerical formulation is stable. The Peclet number (Pe) was less than 1 for $10 \leq Re_h \leq 30$, which means that diffusion dominates in the flow within this range of Reynolds number. At $Re_h \geq 40$, Peclet number was greater than 1, implying that flow is fundamentally convection-dominated.

Table 1: The maximum cell Reynolds number and Courant numbers

Re_h	Maximum Cell Re_h	Maximum Co_u	Maximum Co_v	Maximum Cell Pe
20	27.792	0.00681	0.00124	0.567
30	41.226	0.01010	0.00171	0.841
40	53.647	0.00131	0.00211	1.095
50	62.280	0.01590	0.00245	1.332
100	121.476	0.02980	0.00374	2.479

4. CONCLUSION

The finite-difference formulation is suitable for simulating flow within rectangular channel to visualise velocity distribution and pressure. The solutions obtained through the formulation agree well with benchmark channel flow problem and it satisfies conditions for numerical stability. This present work is able to predict and visualise laminar flow in microchannel, and can be used to capture and analyse convection-diffusion phenomenon in laminar flow through microchannels.

5. ACKNOWLEDGMENT

The authors wish to acknowledge the assistance of the Department of Mechanical Engineering, University of Ibadan, for the provision of the computing facility.

6. CONFLICT OF INTEREST

There is no conflict of interest associated with this work.

REFERENCES

Angenent, L.T. Li, Z., Venkataraman, A. and Rosenbaum, M.A. (2012). A laminar-flow microfluidic device for quantitative analysis of microbial electrochemical activity. *ChemSusChem,* 5, pp. 1119 – 1123.

Batchelor, G. (2000). *Introduction to fluid* mechanics. Cambridge University Press, UK.

Berger, S.A., Talbot, L. and Yao, L.S. (1983). Flow in curved ducts. *Annual Review of Fluid Mechanics, 15*, pp. 461 – 512.

Bode, K., Hooper R.J., Paterson, W.R., Wilson, D.I., Augustin, W. and Scholl, S. (2007). Pulsed flow cleaning of whey protein fouling layers. *Heat Transfer Engineering,* 28, pp. 202-209.

Brandner, J.J., Benzinger, W., Schygulla U., Zimmermann, S. and Schubert, K. (2007). Metallic micro heatexchangers: properties, applications and long term stability. In Heat exchanger fouling and cleaning— VII, Proceedings of Engineering Conferences International (ECI), Tomar, Portugal.

Cengel, Y.A. (2004). *Heat transfer: a practical approach*. 2nd ed. McGraw-Hill, New York.

Fraiwan A., Call, D.F. and Choi, S. (2014). Bacterial growth and respiration in laminar flow microbial fuel cells. *Journal of Renewable and Sustainable Energy,* 6, pp. 1-9.

Jenkins, G. and Mansfield, C.D. (2013). *Microfluidic diagnostics: methods and protocols.* Humana Press.

Kim, B. (2016). An experimental study on fully developed laminar flow and heat transfer in rectangular microchannels. *International Journal of Heat and Fluid Flow,* 62 (Part B), pp. 224-232.

Li, X.J. and Zhou, Y. (2013). *Microfluidic devices for biomedical applications*. Woodhead Publishing, United Kingdom.

Li, Z, Zhang, Y., LeDuc, P.R. and Gregory, K.B. (2011). Microbial electricity generation via microfluidic flow control. *Biotechnology and Bioengineering,* 8(9), pp. 2061 – 2069.

Mees, P.A.J., Nandakumar, K. and Masliyah J.H. (1996). Secondary instability of flow in a curved duct of square cross-section. *Journal of Fluid Mechanics,* 323, pp. 387 – 409.

Morales, R.E.M. and Rosa, E.S. (2012). Modelling fully developed laminar flow in a helical duct with rectangular cross section and finite pitch. *Applied Mathematical Modelling,* 36, pp. 5059 – 5067.

Papadopoulos, P.K. (2011). An auxiliary potential velocity method for incompressible viscous flow. *Journal of Computer and Fluids,* 51, pp. 60 – 69.

Patankar, S.V. and Spalding, D.B. (1972). A calculation procedure for heat, mass and momentum transfer in three dimensional parabolic flows. *International Journal of Heat and Mass Transfer,* 15, pp. 1787-1806.

Qi, X.G., Scott, D.M., and Wilson D.I. (2008). Modelling laminar pulsed flow in rectangular micro-channels. *Journal of Chemical Engineering Science,* 63, pp.2682-2689.

Raja, K.K., Das, M.K., and Kanna, P.R. (2009). Numerical study of mixed convection in a two-dimensional laminar incompressible offset jet flow. *International Journal of Heat and Mass Transfer, 52,* pp. 1023 – 1035.

Sandeep, K.K. (2001). Laminar flow in channels with porous holes, revisited. *Journal of Membrane Science,* 191, pp. 237-241.

Tao, W.Q., Qu, Z.G. and He, Y.L. (2004a). A novel segregated algorithm for incompressible fluid flow and heat transfer problems- CLEAR (Coupled and Linked Equations Algorithm Revised) part I: mathematical formulation and solution procedure. *International Journal Computation and Methodology,* 45(1), pp. 1-17.

Tao, W.Q., Qu, Z.G. and He, Y.L. (2004b). A novel segregated algorithm for incompressible fluid flow and heat transfer problems- CLEAR (Coupled and Linked Equations Algorithm Revised) part II: application examples. *International Journal of Computation and Methodology,* 45(1), pp. 19-48.

Versteeg, H.K. and Malalasekera, W. (2007). *An introduction to computational fluid dynamics: the finite volume method.* 2nd ed. Pearson Education Limited, Edinburgh Gate, England.

Wang, H. and Su, J. (2013). Membraneless microfluidic microbial fuel cell for rapid detection of electrochemical activity of micro-organism. *Bioresource Technology,* 145, pp. 271 – 274.

White, F.M. (1998). *Fluid mechanics*. 4th ed. McGraw-Hill.

Wilson, D.I. (2005). Challenges in cleaning: recent developments and future prospects. *Heat Transfer Engineering,* 26, pp. 51-59.

Zhang, X., Ajaykumar R., Sudhersan, N.M. and Kumar K. (2005). Investigation of 2-d channel flow with a partially compliant wall using finite volume-finite difference approach. *International Journal of Numerical Methods in Fluid,* 49, pp. 635-655.